JACS
JOURNAL OF THE AMERICAN CHEMICAL SOCIETY

Article

pubs.acs.org/JACS

Transient Electrochemical Surface-Enhanced Raman Spectroscopy: A Millisecond Time-Resolved Study of an Electrochemical Redox Process

Cheng Zong,[‡] Chan-Juan Chen,[‡] Meng Zhang, De-Yin Wu, and Bin Ren*

State Key Laboratory of Physical Chemistry of Solid Surfaces, Collaborative Innovation Center of Chemistry for Energy Materials, The MOE Key Laboratory of Spectrochemical Analysis & Instrumentation, Department of Chemistry, College of Chemistry and Chemical Engineering, Xiamen University, Xiamen 361005, China

Supporting Information

ABSTRACT: The pursuit of techniques with a high time resolution together with molecular signature information at the electrochemical interfaces has never stopped in order to explicitly monitor and understand the dynamic electrochemical processes. Here, we developed a transient electrochemical surface-enhanced Raman spectroscopy (TEC-SERS) to monitor the structural evolution of surface species at a time resolution that equals the transient electrochemical methods (e.g., cyclic voltammetry and chronoamperometry), so that the Raman signal with the molecular signature information and the electrochemical current signal can be precisely correlated. The technique was employed to study the redox process of nile blue on Ag surfaces. We revealed an interesting two-rate constant process and a peculiar increase of the absolute intensity during the reduction of nile blue on the Ag surface, which both related to the dissociation of nile blue aggregates and the follow-up reduction. Therefore, we were able to uncover the processes that are impossible to observe by conventional steady state SERS methods. The ability to provide a time resolution shorter than the charging time of the double layer capacitance with molecular fingerprint information has unprecedented significance for investigation of both reversible and irreversible electrochemical processes.

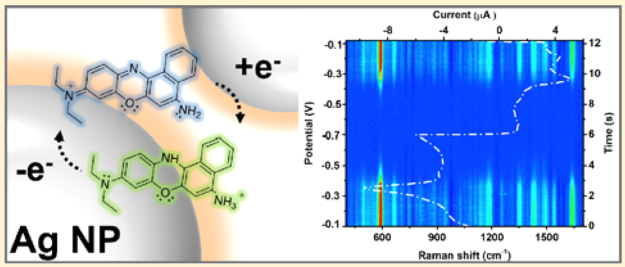

INTRODUCTION

Surface-enhanced Raman spectroscopy (SERS) is a powerful analytical method for surface and interfacial analysis, because it can provide molecular fingerprint information and ultrahigh surface sensitivity.[1] When a surface species is located in the vicinity of plasmonic metal nanostructures and excited with a proper light, the Raman signal of the surface species can be significantly boosted by the enhanced electromagnetic field, even allowing the detection of single molecules.[2] Meanwhile, the near-field feature of the localized surface plasmon resonance (LSPR) enhancement results in the exponential decay of the field strength away from the surface, which can effectively avoid the interference from bulk species.[1a] It should be especially noted that the SERS signal was first observed in an electrochemical system for pyridine adsorbed on a rough silver surface under potential control.[3] Thereafter, electrochemical SERS (EC-SERS) was widely used to characterize electrochemical processes, including interfacial structures, surface reactions, and adsorption of species ranging from small organic and inorganic molecules to large biomolecules on electrodes at different potentials.[1c,4] It has also been extended from noble metal to transition-metal nanostructured surfaces and then to single crystal surfaces.[1d,5]

The common practice of the EC-SERS measurements is to set the electrode potential to a desired value first, then the surface Raman spectra are acquired when the current approaches a stable value. This tactic can be considered a steady-state method and it ensures highly reproducible Raman signals to be obtained. The steady-state method, however, will inevitably lose some important information associated with the transient stage of the interfaces, for example, the induction period of an electrochemical reaction, the relaxation of the interfacial structure, and those coupled to homogeneous chemical reactions in solution.[6] To address these issues, it is necessary to develop EC-SERS techniques that are capable of delineating these processes and exploring the effects of mass transport and charge transfer at a very short time scale. Several time-resolved EC-SERS methods have been developed.[7] One method is a pump−probe based method, in which the electrochemical system was set at an initial potential, then a pump laser beam (or a potential jump) was introduced to the electrochemical system to trigger the molecular system to an "excited" state, and after a short delay time, SERS spectra were acquired with a probe laser.[7a−h] The pump and probe was cycled until a spectrum with a desirable signal-to-noise ratio (SNR) was obtained. The obtained time resolution of the laser pump strategy was determined by the laser pulse, and the spectra were acquired at a fixed potential.[7d,e] Therefore, it can be considered a steady-state method and limited to systems that

Received: July 10, 2015
Published: September 1, 2015

DOI: 10.1021/jacs.5b07197
J. Am. Chem. Soc. 2015, 137, 11768−11774

can be photoactivated to react. In comparison, the potential jump strategy has a more electrochemical implication.[7f−h] It uses a Pockels cell to gate the probe laser which is synchronized with potential jumps to induce electrochemical reactions.[7f−h] Therefore, the time resolution that can be achieved by this method is much shorter than and limited by the response time of the electrochemical cell.[7f] Another method is called the potential-average SERS method, in which an averaged spectrum was acquired while the electrode potential was switched between two potentials at a designed frequency.[7i] By subtracting the averaged spectrum with the spectrum acquired at the initial potential, the time-resolved spectrum of the desired potential can be obtained. In this way, the time-resolved SERS spectra can be obtained on a Raman system without time-resolved capability. The above two methods both require the electrochemical systems to be reversible by the laser excitation or potential modulation. In electrochemistry, potential modulation (potential scan or step) is the most common way to control the electrode processes. If the Raman spectra can be acquired at the same time resolution as the cyclic voltammetry (CV) or chronoamperometry (CA), we would expect to extract rich molecular level information for transient electrochemical processes. The Lombardi group reported a time-resolved EC-SERS (10 ms) of *p*-(hydroxylamino)-nitrobenzoic acid right after switching the electrode to an oxidation potential.[8] They were able to achieve a lifetime of 70 ms for the short-lived intermediates The first and milestone combined SERS and linear voltammetric study of nitrobenzene surface reactions on a SERS-active Au surface was reported by the Weaver group.[9] In that work, they used an integration time of 1−5 s, which is much longer than the dwell time at each potential for a scan rate of 50 mV/s. Therefore, the SERS spectra obtained were indeed the potential average results during the acquisition time. Limited by the availability of an electro-optical instrument at that time, it was extremely challenging for this method to obtain SERS spectra with a good SNR at the millisecond time scale. As a result, the SERS spectra were obtained at a time resolution longer than that of the characteristic time of the transient electrochemical method. The obtained spectra is a time-average or potential-average result, which may lose some detailed molecular information.[10]

In the past two decades, Raman instrumentation is experiencing astonishing improvement in both sensitivity and acquisition time, allowing the use of laser power less than milliwatts for a minimum interference to the system and an acquisition time approaching milliseconds, which is comparable to the charging time of the double-layer capacitance of a normal electrode, especially with the use of an electron multiplying charge coupled device (EMCCD) as a detector. Furthermore, the application of chemometric methods in Raman spectroscopy has further improved the capability to extract useful information from noisy spectra. Therefore, it is timely to reactivate some research activities that have been recognized to be important but difficult to realize 20 years ago. In this work, we developed a transient EC-SERS (TEC-SERS) method by synchronizing a confocal Raman microscope, equipped with a high readout rate EMCCD, with two of the most frequently used electrochemical methods, CV and CA. TEC-SERS is able to provide millisecond time resolution without the repetitive cycled acquisition of the data, which can effectively avoid the averaging effect and retain the transient information. Therefore, it can be used to study both reversible and irreversible systems. To validate the method, we chose nile blue (NB) as a probe molecule. NB is a well-studied pH-dependent cationic phenoxazine dye with a heterocyclic plane, and its redox reaction is a pH-depended quasi-reversible electrode process with two-electron and two-proton transfer at pH < 6.1, as shown in the Supporting Information, Figure S1.[11] In particular, the oxidized form of NB shows a resonance Raman effect and can give a strong Raman signal as shown in Figure S2. Therefore, it has been used in single molecule EC-SERS study to map the local electrochemical potential.[12] We further used a silver nanoparticles (Ag NPs) electrode as a SERS substrate to provide the highest signal. Under such an optimized condition, we were able to perform TEC-SERS study at a time scale that equals the transient electrochemical methods; that is, the acquisition time of each SERS spectrum is comparable to every transient electrochemical data point. We believe such a method will invoke a new surge in the electrochemical application of SERS to unveil the mechanism of some complicated processes.

EXPERIMENTAL SECTION

Preparation of SERS-Active Silver Electrodes. Silver nanoparticles (Ag NP) were prepared according to the classical citrate reduction method of Lee and Meisel, giving a size of about 70−80 nm, as shown in Figure S3.[13] The colloid was concentrated by centrifuge, which was then dropped onto a mechanically polished Ag electrode followed by vacuum drying to obtain the SERS-active Ag NPs electrode. The electrode was then immersed into NB aqueous solution for 2 h, followed by rinsing with plenty of water to remove the physisorbed NB. The electrode was then quickly assembled into a homemade three-electrode electrochemical Raman cell for the in situ SERS measurement. High-purity water (Milli-Q, 18.2 MΩ·cm) was used throughout the study.

TEC-SERS Approach. The detailed experimental procedure was given in Scheme 1 for clarity. All SERS experiments were performed on a WITec confocal Raman microscope. A front-illumination EMCCD (DU970-FI, Andor, readout rate is 2.5 MHz, the maximum number of spectra per second is 649) was used for recording the spectra. Full vertical binning of the CCD pixels was used to achieve a fast readout rate. SERS signals were

Scheme 1. Schematic Illustration of the Setup of TEC-SERS and the Synchronization Sequence of the Trigger[a]

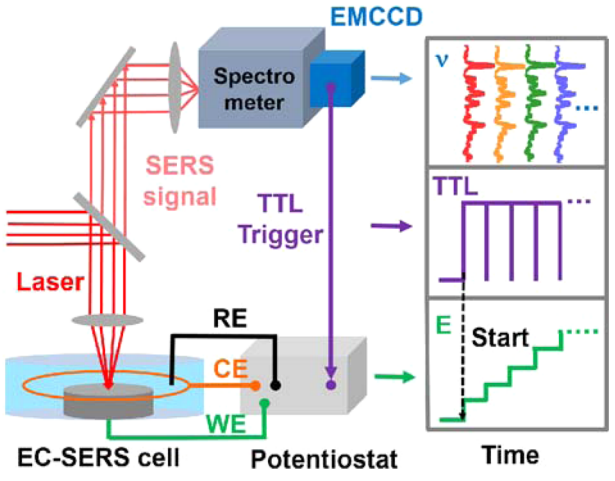

[a]When the EMCCD starts exposure, the TTL signal is generated by the EMCCD and triggers the potentiostat to start a potential sweep.

DOI: 10.1021/jacs.5b07197
J. Am. Chem. Soc. 2015, 137, 11768−11774

excited by 632.8 nm laser with a power density of 1.6×10^5 mW/cm^2 on samples and collected using a 50× objective with an NA of 0.5. The acquisition time is 20 ms for the CV-SERS and 5 ms for the CA-SERS. The potential of the electrode was controlled by a potentiostat (PGSTAT 101, Autolab). All electrode potentials were referred to the saturated calomel electrode (SCE). The CV and CA data were recorded at the same time by the potentiostat during the TEC-SERS measurement. The time interval of the successive data collection in the EMCCD and that of the potentiostat were set to be the same. When the EMCCD is going to expose, a transistor−transistor logic (TTL) signal is generated by the EMCCD. The TTL signal is sent to the potentiostat to initiate the potential sweep. Thereby, the current and spectral data can be exactly synchronized.

Data Analysis. All the spectra shown in this work have been processed by the following methods: cosmic ray removal, Savitzky−Golay smoothing, background subtraction, and wavelet denoise if necessary.[14]

RESULTS AND DISCUSSION

TEC-SERS under Cyclic Voltammetric Control. TEC-SERS was realized by the synchronized SERS and CV measurement of NB adsorbed on a Ag NP electrode in 0.2 M phosphate buffer solution (pH 6). Figure 1a shows the

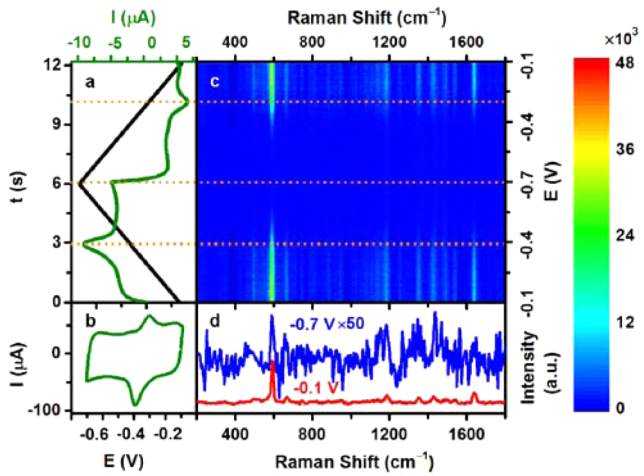

Figure 1. (a) The applied potential waveform (black) and the corresponding current (green) during CV measurement. (b) The CV curve of NB adsorbed on Ag NPs in phosphate buffer (pH 6) recorded at 100 mV/s. (c) The corresponding SERS spectra contour map during the CV measurement. (d) Typical SERS spectra of oxidized (red) and reduced (blue) NB molecules at −0.1 and −0.7 V, respectively.

triangular potential waveform applied to the electrode to obtain the CV, which was triggered by EMCCD. The CV is given in Figure 1b, showing a cathodic peak and an anodic peak at −390 and −302 mV, respectively, with a peak separation of 88 mV. The formal potential can be determined to be −345 mV. The scan rate-dependent result (shown in S4) agrees well with the quasi-reversible redox process of NB. With a commonly used potential sample interval of 2 mV, the dwell time at each potential is 20 ms. The TEC-SERS measurement was performed synchronously during the CV measurement using a same potential interval of 2 mV. The exposure time for every SERS spectrum was about 20 ms in accordance with the CV time interval. The TEC-SERS spectra are presented in Figure 1c as a contour map, in which the *X*-axis is the Raman shift and the *Y*-axis is the time (also the potential), so that the SERS spectral change can be clearly visualized at each potential. For clarity, we plot the CV curve in Figure 1a in the green line for direct comparison of the current response and the spectral response. In accordance with the electrochemical response, the TEC-SERS spectra (Figure 1c) also show a significant but reversible change in intensity when the potential was swept from −0.1 to −0.7 V then back to −0.1 V. To clearly see the spectral feature, we present the SERS spectra of NB in the oxidized (−0.1 V) and reduced (−0.7 V) state in Figure 1d selected from the series of spectra in Figure 1c. The oxidized state of NB (NB_{ox}) is in resonance with the 632.8 nm laser excitation and produces strong resonance Raman signals. Whereas, the reduced state of NB (NB_{red}) is out of resonance and only produces fairly weak signal. In both spectra, the 594 cm^{-1} peak, assigned to the in-plane deformation of the heterocyclic ring (see Table S1 in Supporting Information section S5 for assignment), can be clearly identified, and is sensitive to the potential change. It will be used as a signature peak throughout this work to extract the dynamic information during the transient electrochemical measurement. Limited by the dynamic range of EMCCD, we did not use the EM mode to amplify the SERS signal in the CV-SERS study. In fact, the SNR of the SERS spectra of NB_{ox} and NB_{red} recorded by conventional mode was good enough for further discussion.

From Figure 1c, we can clearly see that the SERS intensity is almost unchanged from 0 to 3 s, when the potential is more positive than the reduction peak potential (−0.39 V). The intensity decreases dramatically and reaches a minimum as the potential is more negative than the reduction peak (from 3 to 6 s). During the period of 5 to 9 s, the SERS signals are barely identified. During the reverse potential scan to the oxidation peak (∼10.5 s), the SERS intensity rapidly increases to its maximum. Similar results were obtained in the CV-SERS studies at different scan rates from 10 to 50 mV/s (as shown in Figure S6). It is of particular significance that every SERS spectrum in the time-evolved SERS spectra and every current point in CV can be well correlated. Therefore, TEC-SERS can reflect the transient information on an electrochemical system with a high fidelity.

An in-depth understanding of the process and the interaction of NB with the Ag surface will be impossible without a clear assignment of all the observed peaks. Assignment of the normal modes of NB is based on the density functional theory (DFT) calculation and also referred to a previous study.[11a] It is essential to note that the spectral feature of the simulated preresonance Raman spectra of the NB_{ox} and the off-resonance Raman spectra of NB_{red} agree well with that of the observed SERS spectra of the adsorbed NB at the oxidation and reduction potential, respectively. The calculation details and related analysis can be found in section S5. To extract the structural information and clarify the change of weak signals of NB_{red}, we present the individual SERS spectra during CV measurement and the zoom-in contour map in the reduction potential range (−0.4 to −0.7 V and then back to −0.4 V) of CV-SERS in Figures S7 and S8, respectively. The characteristic peak of NB_{red} at 1580 cm^{-1} appears at the reduction potential, which confirms the formation of reduced NB at the negative potentials. The peak of NB_{ox} at 1642 cm^{-1} is majorly attributed to NH_2 deformation. A closer comparison of the spectra of the oxidized and reduced NB shows that the peak of NB_{ox} at 1640

DOI: 10.1021/jacs.5b07197
J. Am. Chem. Soc. 2015, 137, 11768−11774

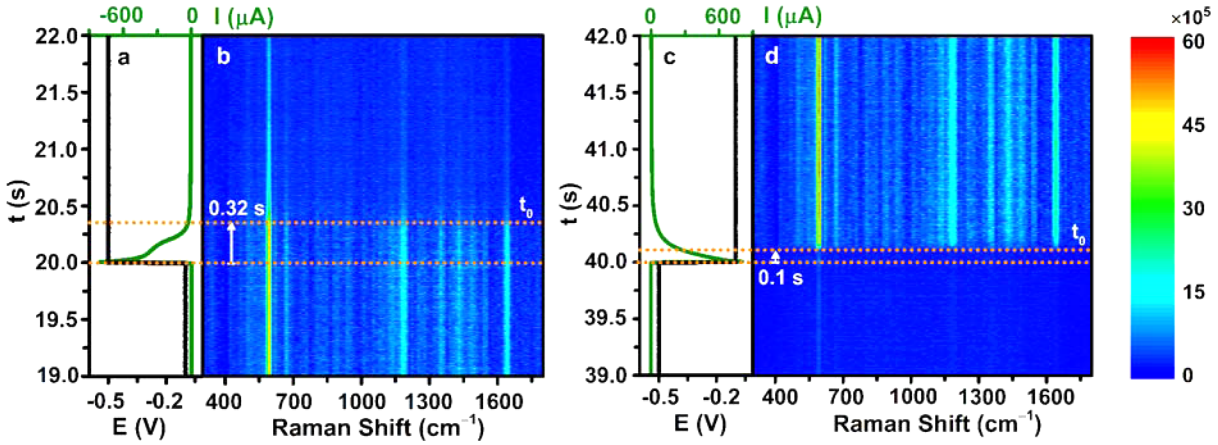

Figure 2. Applied potential waveform and the corresponding current response during the potential jump from −0.1 to −0.5 V (a) then back to −0.1 V (c). Time-resolved SERS contour maps of 10^{-5} M NB adsorbed on the Ag NPs electrode during the reduction (b) and oxidation (d) processes. There are about 0.32 and 0.1 s delay in the change of SERS intensity following the reduction and oxidation potential step, respectively; t_0 is the time that the SERS intensity start to change. The two orange dashed lines in panels b and d define the delay time period of the SERS signal.

cm^{-1} disappears, with the appearance of a new peak at 1636 cm^{-1}. The main reason this occurs is because the NH_2 group is protonated following its reduction. The peak of NB_{red} at 1377 cm^{-1} is mainly assigned to an in-plane C−C stretching mode, and the observation of this peak suggests that the *p*-phenylenediimine group is close to the surface. Therefore, we propose that the aromatic ring plane of NB changes from perpendicular to parallel orientation during the reduction process, which is in accordance with the literature.[11a] The result convincingly demonstrates that the TEC-SERS combined with CV can successfully monitor the fast and detailed structure changes of NB in its redox process, even the weak signals related to the peaks from the NB_{red}, a nonresonant molecule, was observed during the CV measurement.

TEC-SERS for Chronoamperometry (CA). As shown in the Introduction, the traditional way to perform EC-SERS is to step from the initial potential to a desired potential, and the SERS signals are measured until the current approaches a steady-state response. In this way, the obtained SERS signals are highly reproducible. However, this approach misses the transient information concerning the reorganization of the interfacial structure or the induction period of electrochemical reaction. It would be highly desirable if TEC-SERS can also be combined with the CA method, so that the molecular level information can be faithfully obtained during the potential step. The main challenge is that in a CA method the transient processes are usually at the time scale of several milliseconds, roughly in the same order of the double-layer charging time. This time scale requires that the response of the system, both the spectra readout time of the detector and synchronization between the Raman instrument and potentiostat, should be in the order of several milliseconds. On the other hand, a fast response requires a short acquisition time, so that the signal of the system should be strong enough to sustain the SNR of the measurement. To combine with the CA method, we pushed the time resolution (acquisition time) to the readout limit of EMCCD, which is about 5 ms. This acquisition time is much shorter than the charge transfer dynamic time for redox couples involving 2 electrons and 2 protons.[15] It is even shorter than the charging time of double layer capacitance (estimated to be 10 ms) in our system. In such a short acquisition time, the readout noise of CCD becomes the main source of noise and the SERS signal of NB_{red} was overwhelmed by the noise. So we use the EM mode of EMCCD for TEC-SERS detection to overcome the noise, as shown in Figure S9, and reveal the SERS signal of NB. We also introduce a wavelet to denoise without losing any characteristic features in the raw spectrum (as shown in Figure S9).The experiment was performed in a double-step way. The potential of the Ag NPs electrode was first held at an oxidation potential of −0.1 V. Then, it was switched to a reduction potential of −0.5 V. Finally, the potential was switched back to −0.1 V. The potential was held for 20 s after each step. The SERS spectra were acquired with an acquisition time of 5 ms continuously during the whole period of 60 s. Therefore, in total, we obtained 12000 spectra. In fact, the spectral feature and current response became nearly stable after 2 s. We presented in Figure 2 only the spectra and the current−time profile obtained in the last 1 s before the step and the first 2 s after the step. Figure 2a and 2c presents the applied potential profile as well as the current response profile after the application of reduction and oxidization potentials, respectively. In parallel, Figure 2b and 2d show the contour maps of the SERS spectra as a function of time after the potential step. The time-resolved SERS spectra present the evolution of spectra at the beginning of potential step (as shown in S10). From Figure 2a, the current decreases and approaches almost to zero in 0.32 s following the potential step, indicating the complete reduction of NB. However, the SERS spectra start to change after this 0.32 s when the current almost approaches zero, see Figure 2b. Such a delayed response in SERS may be related to the NB aggregates which will be discussed in more detail later. After that, the SERS intensity decreases slowly and remains detectable through the entire reduced process. Figure 2d shows the evolution of the SERS spectra during the potential step to an oxidation potential. In comparison with the 0.32 s delay in the reduction case, the delay time of the SERS response in the oxidation case is 0.1 s following the potential step to the oxidation potential. After another 0.13 s, the SERS signals recover to the same intensity as that in the initial oxidation potential of Figure 2b.

It should be pointed out that the intensity-time profile remains stable even after many potential step cycles, indicating that the slow intensity change during the reduction process is not due to the decomposition of the SERS-active sites, but an

DOI: 10.1021/jacs.5b07197
J. Am. Chem. Soc. 2015, 137, 11768−11774

intrinsic response of the electrode process. Therefore, it may point to a fact that the kinetics of the oxidation process is different from that of the reduction process. To clearly figure out the reason, we plotted the peak intensity of 594 cm^{-1} as a function of time for both the oxidation and reduction processes (see Figure 3 panels a and b). This peak changes synchronously

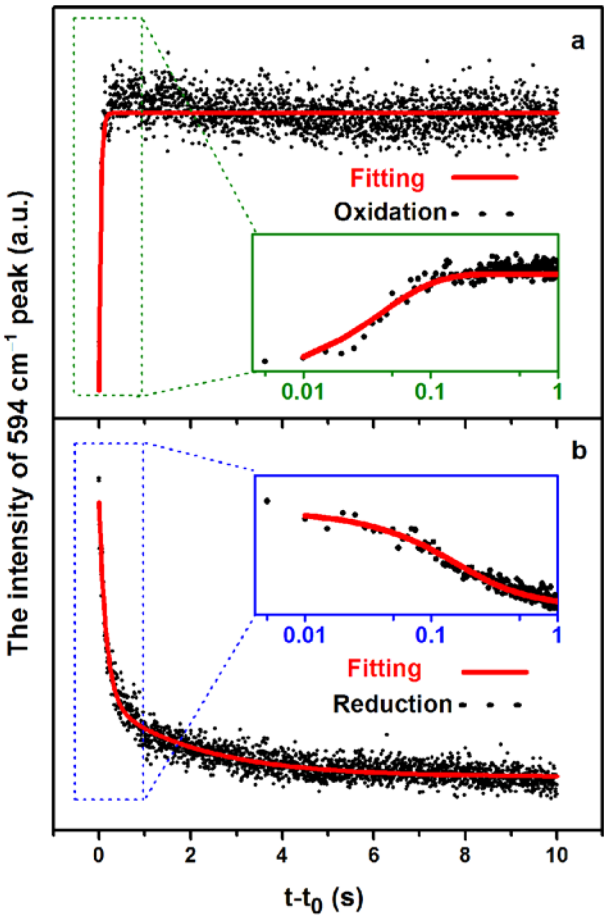

Figure 3. (a) The time-dependent intensity of the SERS peak at 594 cm^{-1} (black scatter plot) during the oxidation process is fitted using a single exponential function (red line) with k_{ox1} = 24.48 ± 1.35 s^{-1}. The inset graph is a zoom-in curve for the data from 0 to 1 s but presented in a log scale to clearly see the changing trend. (b) The time-dependent intensity of the SERS peak at 594 cm^{-1} (black scatter plot) during the reduction process, and the fitted curve using two exponential functions (red line), with k_{red1} = 6.44 ± 0.21 s^{-1} and k_{red2} = 0.48 ± 0.02 s^{-1}. The inset graph is a zoom-in curve from 0 to 1 s. t_0 is the time when the SERS intensity starts to change in the redox process as shown in Figure 2.

with other bands of NB_{ox}, as revealed by the two-dimensional correlation spectroscopy (2DCOS) analysis (as shown in Figure S11). The intensity-time profile of 594 cm^{-1} could reflect the kinetics of the redox process of NB. For this purpose, we fit the curves with exponential functions. Interestingly, the oxidation process can be well fitted with a monoexponential function:

$$I_{ox}(t) = A_{ox}[1 - e^{-k_{ox}(t-t_0)}] + I_{0,ox}$$

Meanwhile, the reduction curve can only be fit well with a two exponential decay functions:

$$I_{red}(t) = A_{red1}e^{-k_{red1}(t-t_0)} + A_{red2}e^{-k_{red2}(t-t_0)} + I_{0,red}$$

The low fitting residual (shown in Figure S12) indicates that the kinetic curves were well fit. The rate constants obtained are k_{ox} = 24.48 ± 1.35 s^{-1} for the oxidation process, and k_{red1} = 6.44 ± 0.21 s^{-1} and k_{red2} = 0.48 ± 0.02 s^{-1} for the reduction process. Here, the k_{red1} agrees well with the reported charge transfer rate (1.4−17 s^{-1}) of adsorbed phenoxazines.[16] The second rate constant k_{red2} is about 13-fold smaller than k_{red1}. We attributed the smaller rate constant to the reaction of NB aggregates on the Ag electrode, which is supported by the UV−vis spectra of NB in PBS solution (pH 6) and the reflectance UV−vis of NB adsorbed Ag NPs electrode shown in the absorption feature of the NB aggregates (as shown in Figure S13). With the formation of aggregates, the proton diffusion involved in the redox process may be slowed down or the charge transfer within the aggregates will decrease.[16b] Considering that only one rate constant was obtained in the oxidation process, the slower proton diffusion may be a more reasonable explanation. The asymmetric response during the oxidation and reduction process of NB further demonstrates the importance to have TEC-SERS to monitor the transient processes at the electrochemical interfaces. This technique is particularly important to those systems involving the structure relaxation, and the proton-coupled electron transfer, which are extremely important to electrocatalysis and other more complex electrochemical systems.

If we increased the NB concentration from 10^{-5} to 10^{-4} M, we found a more interesting phenomenon. Similar to Figure 2, Figure 4 panels a and c show the current response and Figure 4 panels b and d show the time-dependent SERS spectra of NB during the reduction and oxidation processes, respectively. The current response did not show any obvious difference from that at a low concentration of 10^{-5} M, see Figure 2 panels a and c and Figure 4 panels a and c. However, in the time-dependent SERS contour map, we observed an abnormal phenomenon. The SERS spectra obtained at the initial potential (−0.1 V) and the reduction potential (−0.5 V) are still similar to that of the lower NB concentration. However, instead of a decrease in the SERS intensity, an increase of the SERS intensity was observed at the very first 0.41 s upon the potential step to the reduction potential (−0.5 V). This phenomenon is beyond the common sense that the SERS intensity of NB keeps decreasing during its reduction process.[11b,12,15,17] A close examination of other bands of NB reveals that they follow approximately the same trend as 594 cm^{-1}. It is interesting to find in 2DCOS (shown in Figure S11) that 1640 and 594 cm^{-1} peaks are positive crossed in both the synchronous and asynchronous spectra. This result indicates that the intensity of 1640 cm^{-1} changes prior to that of 594 cm^{-1} during the reduction process.[18] It will lead to a decrease of the relative intensity of 1640 and 594 cm^{-1} when the reduction process begins, which can be used as a spectral marker to manifest the reduction process. Therefore, we plotted the SERS intensity of the 594 cm^{-1} and the relative intensity of 1640 cm^{-1}/594 cm^{-1} (abbreviated as 1640/594 ratio) versus time, as shown in Figure 5. After such a data treatment, we found that the 1640/594 ratio decreases instantaneously with the potential change in the reduction process for 10^{-5} M NB. However, with the reduction of NB, the intensity of the SERS spectra becomes too low. Therefore, the ratio curve becomes too noisy to provide any useful information after one second of the reduction process. To clearly see the change, we focus on the very first second during

DOI: 10.1021/jacs.5b07197
J. Am. Chem. Soc. 2015, 137, 11768−11774

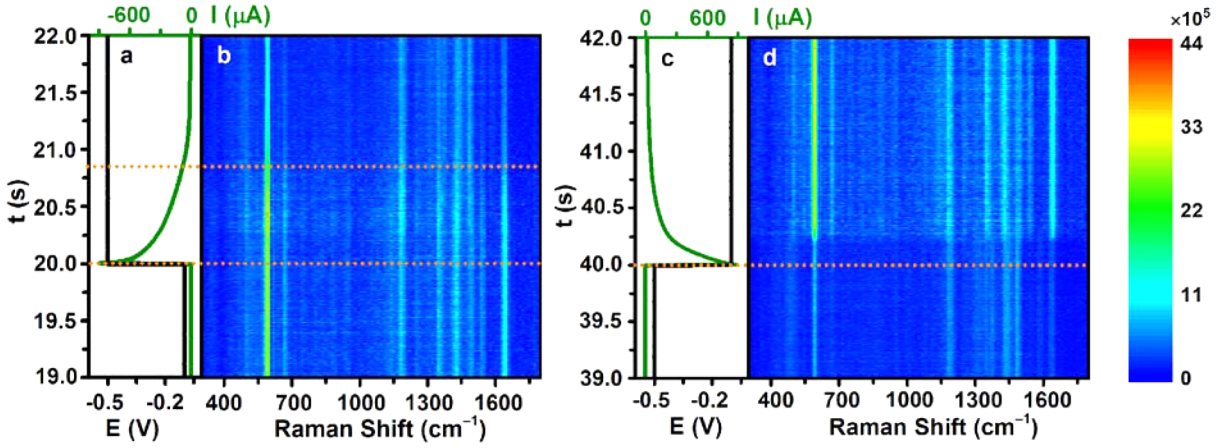

Figure 4. Applied potential waveform and the corresponding current response during the potential jump from −0.1 to −0.5 V (a) and back to −0.1 V (c). Time-resolved SERS contour maps of 10^{-4} M NB adsorbed on the Ag NPs electrode during the reduction (b) and oxidation (d) processes. The two orange dash lines in panel b cover the time period for the appearance of the unexpected increased intensity.

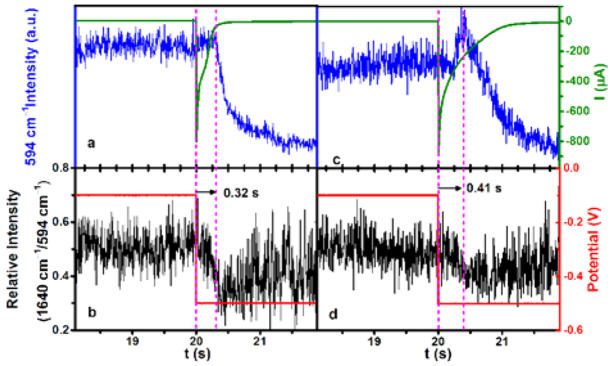

Figure 5. Chronoamperometric curve (green), applied potential waveform (red), time-dependent intensity of the SERS peak at 594 cm^{-1} (blue), and the relative intensity of 1640 cm^{-1}/594 cm^{-1} (black) during the reduction process (−0.1 to −0.5 V) of NB adsorbed from the solution containing 10^{-5} M (a, b) and 10^{-4} M (c, d) NB.

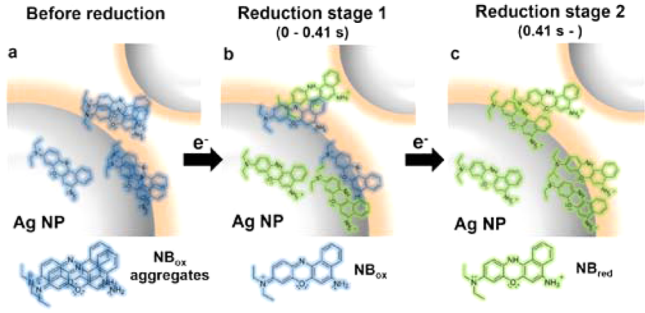

Figure 6. Scheme of the reduction process of NB on Ag NPs. (a) Before the application of the reduction potential, the NB_{ox} monomer and H-aggregates both exist on Ag NPs. (b) The monomer is reduced leading to the decrease of the SERS signal, and the aggregates are dissociated leading to an enhanced SERS signal. This stage is denoted as stage 1. (c) After most of the NB_{ox} aggregates have been dissociated, the remained NB_{ox} monomers keep reducing and the SERS intensity decreases, which is denoted as stage 2.

the reduction of 10^{-4} M NB. We divide the reduction process shown in Figure 5c,d into two stages based on the intensity and relative intensity change. In the first 0.41 s after the potential step to a reduction potential, the intensity of 594 cm^{-1} increases to the maximum, while the 1640/594 ratio keeps decreasing. From 0.41 to 1 s after the potential step, the intensity of 594 cm^{-1} and the 1640/594 ratio both decrease.

This peculiar trend of the absolute intensity of NB_{ox} change during the reduction process is a highly reproducible phenomenon, which indicates that there is an intrinsic origin for it. We that propose such a concentration-dependent phenomenon is related to the electrochemical reaction of both the NB_{ox} monomer and H-aggregates on the surface.[19] To clearly illustrate the reaction process under the high NB_{ox} concentration, we propose a scheme to illustrate the reaction process in Figure 6. To understand the phenomenon clearly, we keep in mind that NB_{ox} monomer is in good resonance with the laser, the NB_{red} monomer is off-resonance, and the NB_{ox} aggregate is preresonant with the laser. It indicates that a same amount of NB molecule will produce signal intensity following the order NB_{ox} > NB_{ox} aggregate > NB_{red}. At the oxidation potential, both the NB_{ox} monomers and small NB_{ox} aggregates are present on the surface. When the potential is moved to the reduction potential, the NB_{ox} monomer is reduced to NB_{red}, leading to a decrease of the SERS signal. Meanwhile, some NB_{ox} in the aggregates in good contact with the surface will also be partially reduced to form NB_{red}, leading to the dissociation of aggregates and the formation of NB_{ox} monomers (see Figure 6b and Figure S13c).[20] The newly formed NB_{ox} monomers produce a stronger signal than when they are in aggregates. Therefore, the SERS signal will increase before the reduction of the remaining NB_{ox} monomers. When most of the aggregates have been dissociated, the SERS intensity will reach its maximum. Then in the second stage, the reduction of the remaining NB_{ox} monomers lead to the decreased NB signal (Figure 6c). The absolute intensity increase lasts less than 1 s. A similar process may also explain the delay time of the reduction process of 10^{-5} M NB, as the decreased intensity during the reduction process is compensated by the increased contribution of the dissociated NB_{ox} molecule. Therefore, it is reasonable that there is a delay in the SERS response as compared with the current response (as shown in Figures 2b and 5a). The reverse process of the dissociation of NB_{ox} leads to the delay time in the oxidized process.

Our dynamic result indicates TEC-SERS can detect a transient relaxation of interfacial structure, investigate the whole process with a time resolution of 5 ms, and perform the whole process in detail. Further systematic work is required for

DOI: 10.1021/jacs.5b07197
J. Am. Chem. Soc. 2015, 137, 11768−11774

an explicit understanding of the dynamic process of the interfacial structure.

CONCLUSION

In summary, we have developed a transient electrochemical surface-enhanced Raman spectroscopy (TEC-SERS) for studying the evolution of the molecular structure during the redox process. TEC-SERS benefits from recent advances in electro-optical instruments and data postprocessing and can obtain SERS spectra at a high time resolution with a good SNR without the limit of a reversible system. Since each electrochemical datum has its corresponding spectrum in TEC-SERS, this technique allows us to monitor the detailed molecular changes in a continuous way and to obtain kinetic information on the redox process. We revealed an unexpected two-rate constant process and a peculiar absolute intensity increasing stage occurring at the time scale of less than a second occurring for the reduction of nile blue on the Ag surface with this method, which is not possible for conventional steady state SERS methods to discriminate. The ability to provide molecular signature information under in situ electrochemical control at a time resolution shorter than the charging time of the double layer capacitance for both reversible and irreversible electrochemical processes is of high significance for electrochemistry, especially for that involving the transient structure relaxation, and the proton-coupled electron transfer. Such a success will further invoke the future incorporation of advanced electro-optical instruments (e.g., the high-throughput virtual slit, the EM-ICCD, and the water immersing objective with a high NA) and nanostructures with a better SERS enhancement into TEC-SERS, which may further push the time resolution to submilliseconds or even submicroseconds for investigation of even faster electrochemical processes.

ASSOCIATED CONTENT

Supporting Information

The Supporting Information is available free of charge on the ACS Publications website at DOI: 10.1021/jacs.5b07197.

Additional figures and tables; DFT computational details (PDF)

AUTHOR INFORMATION

Corresponding Author

*bren@xmu.edu.cn

Author Contributions

‡C.Z. and C.-J.C. contributed equally

Notes

The authors declare no competing financial interest.

ACKNOWLEDGMENTS

We acknowledge support from NSFC (21227004, 21321062, and J1310024), MOST (2013CB933703 and 2011YQ03012406), and MOE (IRT13036).

REFERENCES

(1) (a) Wu, D.-Y.; Li, J.-F.; Ren, B.; Tian, Z.-Q. *Chem. Soc. Rev.* **2008**, *37*, 1025−1041. (b) Schlucker, S. *Angew. Chem., Int. Ed.* **2014**, *53*, 4756−4795. (c) Tian, Z.-Q.; Ren, B. *Annu. Rev. Phys. Chem.* **2004**, *55*, 197−229. (d) Tian, Z.-Q.; Ren, B.; Wu, D.-Y. *J. Phys. Chem. B* **2002**, *106*, 9463−9483.

(2) (a) Kneipp, K.; Wang, Y.; Kneipp, H.; Perelman, L. T.; Itzkan, I.; Dasari, R.; Feld, M. S. *Phys. Rev. Lett.* **1997**, *78*, 1667−1670. (b) Nie, S. M.; Emery, S. R. *Science* **1997**, *275*, 1102−1106. (c) Le Ru, E. C.; Etchegoin, P. G. *Annu. Rev. Phys. Chem.* **2012**, *63*, 65−87. (d) Sonntag, M. D.; Klingsporn, J. M.; Zrimsek, A. B.; Sharma, B.; Ruvuna, L. K.; Van Duyne, R. P. *Chem. Soc. Rev.* **2014**, *43*, 1230−1247.

(3) (a) Fleischmann, M.; Hendra, P. J.; McQuillan, A. *Chem. Phys. Lett.* **1974**, *26*, 163−166. (b) Jeanmaire, D. L.; Van Duyne, R.P. J. *J. Electroanal. Chem. Interfacial Electrochem.* **1977**, *84*, 1−20.

(4) (a) Ambrosio, R. C.; Gewirth, A. A. *Anal. Chem.* **2010**, *82*, 1305−1310. (b) Dick, L. A.; Haes, A. J.; Van Duyne, R. P. *J. Phys. Chem. B* **2000**, *104*, 11752−11762. (c) Huang, Y. F.; Zhang, M.; Zhao, L. B.; Feng, J. M.; Wu, D. Y.; Ren, B.; Tian, Z. Q. *Angew. Chem., Int. Ed.* **2014**, *53*, 2353−2357.

(5) (a) Kwon, H.; Gewirth, A. A. *J. Electrochem. Soc.* **2007**, *154*, D577−D583. (b) Yang, H.; Yang, Y.; Zou, S. *J. Phys. Chem. C* **2007**, *111*, 19058−19065. (c) Weaver, M. J.; Zou, S.; Chan, H. Y. H. *Anal. Chem.* **2000**, *72*, 38A−47A. (d) Hu, J. W.; Chen, S.; Johnson, R. P.; Lin, X. D.; Yang, Z. L.; Russell, A. E. *J. Phys. Chem. C* **2013**, *117*, 24843−24850.

(6) Bard, A. J.; Stratmann, M. *Encyclopedia of Electrochemistry*; Wiley-VCH: 2002−2007.

(7) (a) Bell, S. *Analyst* **1996**, *121*, 107−120. (b) Shi, C. T.; Zhang, W.; Birke, R. L.; Lombardi, J. R. *J. Electroanal. Chem.* **1997**, *423*, 67−81. (c) Zhang, W.; Vivoni, A.; Lombardi, J. R.; Birke, R. L. *J. Phys. Chem.* **1995**, *99*, 12846−12857. (d) Shi, C.; Zhang, W.; Lombardi, J. R.; Birke, R. L. *J. Phys. Chem.* **1992**, *96*, 10093−10096. (e) Misono, Y.; Shibasaki, K.; Yamasawa, N.; Mineo, Y.; Itoh, K. *J. Phys. Chem.* **1993**, *97*, 6054−6059. (f) Murgida, D. H.; Hildebrandt, P. *J. Am. Chem. Soc.* **2001**, *123*, 4062−4068. (g) Wackerbarth, H.; Klar, U.; Gunther, W.; Hildebrandt, P. *Appl. Spectrosc.* **1999**, *53*, 283−291. (h) Murgida, D. H.; Hildebrandt, P. *Angew. Chem., Int. Ed.* **2001**, *40*, 728−731. (i) Tian, Z.; Li, W.; Mao, B.; Zou, S.; Gao, J. *Appl. Spectrosc.* **1996**, *50*, 1569−1577.

(8) Shi, C.; Zhang, W.; Birke, R. L.; Lombardi, J. R. *J. Phys. Chem.* **1990**, *94*, 4766−4769.

(9) Gao, P.; Gosztola, D.; Weaver, M. J. *J. Phys. Chem.* **1988**, *92*, 7122−7130.

(10) (a) Santos, D.P.d.; Andrade, G. F.; Temperini, M. L.; Brolo, A. G. *J. Phys. Chem. C* **2009**, *113*, 17737−17744. (b) Blackie, E.; Le Ru, E.; Meyer, M.; Timmer, M.; Burkett, B.; Northcote, P.; Etchegoin, P. *Phys. Chem. Chem. Phys.* **2008**, *10*, 4147−4153.

(11) (a) Ni, F.; Feng, H.; Gorton, L.; Cotton, T. M. *Langmuir* **1990**, *6*, 66−73. (b) Cortés, E.; Etchegoin, P. G.; Le Ru, E. C.; Fainstein, A.; Vela, M. E.; Salvarezza, R. C. *J. Am. Chem. Soc.* **2013**, *135*, 2809−2815.

(12) Wilson, A. J.; Willets, K. A. *Nano Lett.* **2014**, *14*, 939−945.

(13) Lee, P. C.; Meisel, D. *J. Phys. Chem.* **1982**, *86*, 3391−3395.

(14) (a) Zhang, Z.-M.; Chen, S.; Liang, Y.-Z. *Analyst* **2010**, *135*, 1138−1146. (b) Feuerstein, D.; Parker, K. H.; Boutelle, M. G. *Anal. Chem.* **2009**, *81*, 4987−4994.

(15) Cortés, E.; Etchegoin, P. G.; Le Ru, E. C.; Fainstein, A.; Vela, M. E.; Salvarezza, R. C. *J. Am. Chem. Soc.* **2010**, *132*, 18034−18037.

(16) (a) Ju, H.; Ye, Y.; Zhu, Y. *Electrochim. Acta* **2005**, *50*, 1361−1367. (b) Malinauskas, A.; Ruzgas, T.; Gorton, L. *J. Electroanal. Chem.* **2000**, *484*, 55−63. (c) Huck, H. *Phys. Chem. Chem. Phys.* **1999**, *1*, 855−859.

(17) Cortés, E.; Etchegoin, P. G.; Le Ru, E. C.; Fainstein, A.; Vela, M.a.E.; Salvarezza, R. C. *Anal. Chem.* **2010**, *82*, 6919−6925.

(18) Noda, I.; Ozaki, Y. *Two-Dimensional Correlation Spectroscopy: Applications in Vibrational and Optical Spectroscopy*; John Wiley & Sons: 2005.

(19) Huang, C. Z.; Li, Y. F.; Zhang, D. J.; Ao, X. P. *Talanta* **1999**, *49*, 495−503.

(20) Lenhard, J. R.; Hein, B. R. *J. Phys. Chem.* **1996**, *100*, 17287−17296.

DOI: 10.1021/jacs.5b07197
J. Am. Chem. Soc. 2015, 137, 11768−11774